Transfer Functions for Series of Continuously Stirred Biofilm Reactors[1]

Torsten Wik and Claes Breitholtz
Control Engineering Laboratory
Chalmers University of Technology
S-412 96 Göteborg, Sweden

email: tw@control.chalmers.se, cb@control.chalmers.se

[1]Technical Report CTH/RT/I-97/001 (May 20, 1997)

Abstract

There is an increasing interest in modeling and applications of biofilm reactors. Commonly, biofilm reactors are modeled as a single continuously stirred biofilm reactor (CSBR), or as a series of such. The models can be used to extract information about the reactor, for design and to predict reactor effluent characteristics as a function of influent characteristics. A CSBR consists of a stirred tank, which the bulk water flows through, and from which substrates diffuse into a biofilm where they may be transformed into new substances by bacteria living in the biofilm. Here, standard assumptions are used to derive a general and flexible dynamic model of CSBR-systems, where the reaction kinetics are of zero or first order. An exact, and an approximate transfer function, which enables easy simulations, analysis, and implementation in real-time softwares, is derived. Particular focus is on pulse responses, which is an important experimental procedure in control and reactor design. Explicit equations for the pulse responses are presented, and parameter dependancy is discussed. Experimental data from a pilot plant nitrifying trickling filter are used to illustrate the use of transfer functions for identification of reactor and biofilm parameters.

Keywords: Biofilm, diffusion, dynamics, identification, modeling, pulse response, reactor, residence time, transfer function, trickling filter, wastewater.

Contents

1 Introduction

Fixed biofilms can be characterized as an organic matrix attached to a substratum. In biofilm reactors the bacterial populations inside such organic matrices are used for carrying out transformations of some specific substances into other substances.

One field, where biofilm reactors have attained increased attention, is potable and wastewater treatment. They are particularly popular for nitrogen reduction since, due to the low growth rates of nitrifiers, the nitrifying population may be washed from reactors with suspended bacteria.

A nitrifying trickling filter is an example of such biofilm reactors. Others are: rotating biological contactors, biofilters and KMT-processes. Those can be modeled as a single continuously stirred biofilm reactor (CSBR), or a series of CSBRs. Each CSBR is modeled as a continuously stirred tank (CST) communicating with a biofilm compartment (BFC) by diffusion into and out of the biofilm. This approach has been widely used in modeling of biofilm reactors during the last decades [4, 6, 7, 9]. The described modeling approach is illustrated in Figure 1, where c^b is the substrate bulk concentrations in the CSTs, J is the flux into (positive) and out of (negative) the biofilm, Q is the flow through the reactor, and V is the total bulk water volume in the reactor.

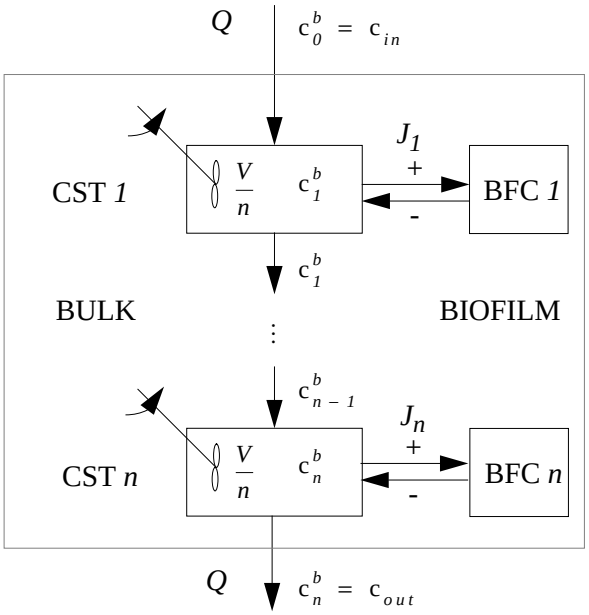

Figure 1: Illustration of the modeling approach.

2 Notation

A	total area of biofilm in the reactor (m^2)
C, c	substrate concentration inside the biofilm (gm^{-3} or no dim.)
C^b, c^b	substrate concentration in the bulk liquid (gm^{-3} or no dim.)
c_δ	concentration pulse coefficient (gm^{-3} or no dim.)
D	substrate diffusivity within the biofilm (m^2d^{-1})
d	Taylor expansion coefficients for $F(s)$
F	denumerator of transfer function
f	Taylor expansion coefficients for $F(s)^n$
G	transfer function
J	substrate flux into biofilm ($gm^{-2}d^{-1}$)
k_s	Monod saturation coefficient (gm^{-3})
L	biofilm thickness (m)
m	number of singularities considered
m_δ	mass of trace substance added to the reactor (g)
M	number of discretization points
n	number of CSBRs in series
Q	flow through the reactor (m^3d^{-1})
R, r	specific reaction rate (no dim.), (d^{-1})
s	Laplace variable
t, $\bar{t}$	time (no dim.), (d)
V	total bulk liquid volume in the reactor (m^3)
X	bacterial concentration in the biofilm ($gCODm^{-3}$)
x, $\bar{x}$	distance in the biofilm from the substratum (no dim.), (m)
Y	biomass yield coefficient ($gCODg^{-1}$)

Greek letters

α	singularities of the transfer function
ϵ	volume fraction of water in biofilm (m^3m^{-3})
κ	dimensionless first order rate coefficient
μ_m	maximum specific growth rate (d^{-1})
τ	dimensionless time constant
γ	dimensionless biofilm flux coefficient

3 Modeling

It should be stressed that in the modeling and analysis that follow, if not otherwise pointed out, the biofilm reactor is divided into n equal CSBRs. This is an abundant assumption, made only for easier notation and clearer analysis. Every CSBR can be modeled independently of each other, i.e. biofilm thickness, diffusion coefficients, biofilm porosity, volume of bulk water, biofilm area, reaction rate, kinetics and stoichiometry can be modelled independently for each CSBR. The methods and analysis will remain the same, but since they cannot be carried out in dimensionless time in a straight forward manner, indexing and expressions become rather cumbersome.

With the modeling approach illustrated in Figure 1, a mass-balance over each CST gives

$$(V/n)\frac{d}{d\bar{t}}c_j^b = Q(c_{j-1}^b - c_j^b) - J_j, \qquad j = 1, 2 \ldots n. \tag{1}$$

Note that time is denoted by $\bar{t}$ instead of t, which will be used to denote dimensionless time.

Each biofilm compartment (BFC) is modeled as a biofilm with a surface area A/n, where A is the total area of biofilm in the reactor. The following assumptions are made in the modeling of the BFCs:

A1. All substrate concentrations in the biofilm are continuous.

A2. The fraction of water in the biofilm (ϵ), the substrate diffusion coefficient (D), and the biofilm thickness (L) are assumed constant.

A3. The transport of substrates inside the biofilm obeys Fick's law of diffusion in one dimension.

A4. There is no diffusion resistance between the bulk and the biofilm.

A5. The bacterial concentrations in the BFCs are constant in time, but may vary with depth in the biofilm.

As mentioned, assumption A2 can be relaxed such that V, A, ϵ, D, and L are constant in each CSBR, but not equal in all CSBRs.

We begin by modeling a reactor where no reaction takes place in the biofilm, and then show that this is equivalent to when a reaction of zero order kinetics takes place in the biofilm.

Assumption A1 to A3 can be used to describe the substrate concentrations inside a non-reacting biofilm by a mass-balance:

$$\epsilon \frac{\partial c_j}{\partial \bar{t}} = D \frac{\partial^2 c_j}{\partial \bar{x}^2}, \qquad 0 < \bar{x} < L, \qquad j = 1, 2 \ldots n, \tag{2}$$

where D is the diffusion coefficient for the substrate considered in the biofilm. Note that the distance from the biofilm substratum is denoted $\bar{x}$, since x will denote the corresponding dimensionless variable.

Two boundary conditions are needed for eqn. (2). The first is a consequence of the fact that no substrate is diffusing through the substratum, and the second is a result of assumption A4:

$$\frac{\partial}{\partial \bar{x}} c_j(0, \bar{t}) = 0, \qquad c_j(L, \bar{t}) = c_j^b(\bar{t}), \qquad j = 1, 2 \ldots n. \tag{3}$$

The substrate flux linking eqn. (1) for the bulk, and eqn. (2) for the biofilm can be expressed as:

$$J_j(\bar{t}) = (A/n) D \frac{\partial}{\partial \bar{x}} c_j(L, \bar{t}), \qquad j = 1, 2 \ldots n, \tag{4}$$

due to assumptions A1 to A3.

In the analysis to follow, it facilitates to use the equations in a dimensionless form. Therefore, we introduce the following scaling of the time $\bar{t}$ and the distance $\bar{x}$ from the substratum:

$$t = \frac{D}{L^2 \epsilon} \bar{t} \quad \text{and} \quad x = \frac{\bar{x}}{L} \tag{5}$$

Eqn. (1), combined with (4), then takes the form

$$\frac{VD}{nL^2\epsilon} \frac{d}{dt} c_j^b(t) = Q(c_{j-1}^b(t) - c_j^b(t)) - \frac{AD}{nL} \frac{\partial}{\partial x} c_j(1, t). \tag{6}$$

If we let

$$\tau = \frac{VD}{nL^2 \epsilon Q} \quad \text{and} \quad \gamma = \frac{AD}{nQL},$$

eqn. (6) cah be rewritten as

$$\tau \frac{d}{dt} c_j^b(t) = c_{j-1}^b(t) - c_j^b(t) - \gamma \frac{\partial}{\partial x} c_j(1, t). \tag{7}$$

In the dimensionless form eqn. (2) becomes

$$\frac{\partial}{\partial t} c_j(x, t) = \frac{\partial^2}{\partial x^2} c_j(x, t), \qquad 0 < x < 1. \tag{8}$$

Eqns. (7) and (8) can be shown to also model a biofilm where reaction of the substrate takes place in the biofilm. A reaction term is then added to the mass-balance (2):

$$\epsilon \frac{\partial c_j}{\partial \bar{t}} = D \frac{\partial^2 c_j}{\partial \bar{x}^2} - r_j(\bar{x}, c_j), \qquad 0 < \bar{x} < L, \qquad j = 1, 2 \ldots n, \tag{9}$$

where r_j is the volumetric specific rate of reaction.

The dimensionless equivalence of eqn. (9) then becomes

$$\frac{\partial c_j}{\partial t} = \frac{\partial^2 c_j}{\partial x^2} - R_j(x, c_j), \qquad 0 < x < 1, \qquad j = 1, 2 \ldots n, \tag{10}$$

where $R_j = (L^2/D) r_j$.

The rate of reaction is commonly modeled by zero or first order kinetics, or by a Monod-expression

$$r_j(x, c_j) = X_j(x) \frac{\mu_m}{Y} \frac{c_j}{k_s + c_j}, \tag{11}$$

where X is the bacterial concentration, which may vary with distance x from the substratum, Y is the yield coefficient of the bacteria, μ_m is the maximum growth rate of the bacteria, and k_s is the Monod saturation coefficient. The Monod-expression can be seen as a transition from first order to zero order kinetics with increasing substrate concentration.

Zero order kinetics

At high substrate concentrations the rate expression (11) can be assumed of zero order:

$$R_j(x) = X_j(x) \frac{\mu_m L^2}{YD}, \quad 0 < x < 1.$$

By differentiation, it can be verified that the stationary solutions to eqns. (7) and (10) are

$$\bar{c}_j^b = \bar{c}_0^b - \gamma \sum_{k=1}^{j} \int_0^1 R_k(z) dz, \quad j = 1, 2, \ldots n, \tag{12}$$

$$\bar{c}_j(x) = \bar{c}_0^b - \gamma \sum_{k=1}^{j} \int_0^1 R_k(z) dz - \int_x^1 \int_0^y R_j(z) dz dy, \quad j = 1, 2, \ldots n, \tag{13}$$

where $\bar{c}_0^b$ is the influent concentration. It is easy to verify by insertion that eqns. (7) and (8) with boundary conditions (3), and zero initial conditions describe the deviations

$$\tilde{c}_j^b(t) = c_j^b(t) - \bar{c}_j^b \quad \text{and} \quad \tilde{c}_j(x, t) = c_j(x, t) - \bar{c}_j(x) \tag{14}$$

from the stationary solutions. Hence, the problem with no reaction and the problem with zero order reaction are equivalent from a dynamic point of view. Note that eqn. (12) implies that the spatial distribution of the reaction rate in the biofilm does not affect the influent/effluent behavior. Further, only the sum of reaction rates integrated over the biofilm in each CSBR, i.e. the mean reaction rate, will affect the level of the effluent. However, it does not affect the dynamics.

First order kinetics

At low substrate concentrations the rate expression (11) can be assumed of first order:

$$r_j(c_j) = \frac{X\mu_m}{Yk_s}c_j.$$

Denoting $(X\mu_m L^2)/(Yk_sD)$ by κ, eqn. (10) becomes

$$\frac{\partial}{\partial t}c_j(x,t) = \frac{\partial^2}{\partial x^2}c_j(x,t) - \kappa c_j(x,t). \tag{15}$$

The stationary solutions to eqns. (15) and (7) now become

$$\begin{aligned}
\bar{c}_j^b &= \bar{c}_0^b \frac{1}{(1+\gamma\sqrt{\kappa}\tanh(\sqrt{\kappa}))^j}, \quad j = 1, 2, \ldots n \\
\bar{c}_j(x) &= \bar{c}_0^b \frac{\cosh(\sqrt{\kappa}x)}{\cosh(\sqrt{\kappa})(1+\gamma\sqrt{\kappa}\tanh(\sqrt{\kappa}))^j}, \quad j = 1, 2, \ldots n.
\end{aligned}$$

4 Exact transfer function

The exact transfer function from influent to effluent concentration will be derived for first order kinetics. However, by letting κ in eqn. (15) be zero we get the case of no reaction, which has been shown to be equivalent to zero order reaction. Hence, the transfer function will hold for all these cases.

Assuming initial stationary conditions, Laplace transformation of eqn. (7) gives

$$\tau s C_j^b(s) = C_{j-1}^b(s) - C_j^b(s) - \gamma\frac{d}{dx}C_j(1,s), \tag{16}$$

where all transformed variables now represent the deviations (14) from initial equilibrium values, i.e., $C_j^b(s) = \mathcal{L}\{\tilde{c}_j^b(t)\}$ and $C_j(x,s) = \mathcal{L}\{\tilde{c}_j(x,t)\}$.

Laplace transformation of eqn. (15) gives

$$sC_j(x,s) = \frac{d^2}{dx^2}C_j(x,s) - \kappa C_j(x,s), \qquad 0 < x < 1,$$

which has the solution

$$C_j(x,s) = A(s)\cosh(x\sqrt{s+\kappa}) + B(s)\sinh(x\sqrt{s+\kappa}).$$

Since

$$\frac{d}{dx}C_j(x,s) = A(s)\sqrt{s+\kappa}\sinh(x\sqrt{s+\kappa}) + B(s)\sqrt{s+\kappa}\cosh(x\sqrt{s+\kappa}) \tag{17}$$

and the Laplace transforms of the boundary conditions (3) are

$$\frac{d}{dx}C_j(0,s) = 0 \quad \text{and} \quad C_j(1,s) = C_j^b(s),$$

it follow that

$$A(s) = \frac{C_j^b(s)}{\cosh(\sqrt{s+\kappa})} \quad \text{and} \quad B(s) = 0.$$

Inserting these, first into eqn. (17), and then the result into eqn. (16), gives

$$\tau s C_j^b(s) = C_{j-1}^b(s) - C_j^b(s) - \gamma \frac{C_j^b(s)}{\cosh(\sqrt{s+\kappa})}\sqrt{s+\kappa}\sinh(\sqrt{s+\kappa}).$$

Hence, the transfer function for each CSBR satisfies

$$\begin{aligned} G_j(s) &= \frac{C_j^b(s)}{C_{j-1}^b(s)} \\ &= \frac{1}{1+\tau s + \gamma\sqrt{s+\kappa}\tanh(\sqrt{s+\kappa})} \\ &= \frac{K}{1+\tilde{\tau}(s+\kappa) + \tilde{\gamma}\sqrt{s+\kappa}\tanh(\sqrt{s+\kappa})}, \end{aligned} \tag{18}$$

where $K = 1/(1-\tau\kappa)$, and $\tilde{\tau} = K\tau$ and $\tilde{\gamma} = K\gamma$. Note that independantly of the kinetics $\tilde{\tau}$ and $\tilde{\gamma}$ always have the same sign, and that if $\tau\kappa > 1$ then they are negative. Further, if $\kappa = 0$ (no reaction or zero order kinetics) we have $K = 1$, $\tilde{\tau} = \tau$ and $\tilde{\gamma} = \gamma$.

The transfer function describing the influent/effluent behavior becomes:

$$\begin{aligned} G(s) &= \frac{C_{out}(s)}{C_{in}(s)} \\ &= \frac{K^n}{(1+\tilde{\tau}(s+\kappa) + \tilde{\gamma}\sqrt{s+\kappa}\tanh(\sqrt{s+\kappa}))^n}. \end{aligned} \tag{19}$$

If the reactor is not divided into equal CSBRs each $G_j(s)$ is different and $G(s)$ is the product of all $G_j(s)$.

5 Singularities of the transfer function

The singularities of the derived transfer function must be determined in order to use the transfer function to calculate dynamic responses to changes in influent conditions in the time domain. First, we will show that all singularities to $G_j(s)$, and, hence, also $G(s)$, are on the negative real axis. Then, the singularities of $G(s)$, and their multiplicity, may easily be found.

Let

$$z = \sqrt{s+\kappa} \quad \Leftrightarrow \quad s = z^2 - \kappa$$

The denominator of $G_j(s)$ then becomes

$$1 + \tilde{\tau} z^2 + \tilde{\gamma} z \tanh z,$$

The singular points of G_j are given by the characteristic equation

$$1 + \tilde{\tau} z^2 + \tilde{\gamma} z \tanh z = 0. \tag{20}$$

Writing the complex variable z as $x + iy$, and using the fact that

$$\tanh z = \frac{\sinh 2x}{\cosh 2x + \cos 2y} + i \frac{\sin 2y}{\cosh 2x + \cos 2y},$$

the imaginary part of eqn. (20) divided by $\tilde{\tau}$ becomes

$$2xy + \frac{\tilde{\gamma}}{\tilde{\tau}} \cdot \frac{x \sin 2y + y \sinh 2x}{\cosh 2x + \cos 2y} = 0.$$

This eqn. is the sum of two terms having the same sign as xy. Hence, all solutions to eqn. (20) must be either on the imaginary axis or on the real axis. Since the origin impossibly can be a solution, the solutions on the real axis are given by

$$\tilde{\gamma} \tanh x = -(\tilde{\tau} x + 1/x) \tag{21}$$

For zero order kinetics, or no reaction at all, this equation has no solution since positive $\tilde{\tau}$ and $\tilde{\gamma}$ imply opposite signs of the left and right hand side. However, for first order kinetics, when $\tilde{\tau}$ and $\tilde{\gamma}$ are negative, there will always be two solutions centered around $x = 0$. In Figure 2 the locations of the solutions are illustrated for $\tilde{\tau} = -1$ and $\tilde{\gamma} = -1$.

For negative $\tilde{\tau}$ and $\tilde{\gamma}$, the right hand side of eqn. (21) equals zero for $x = 1/\sqrt{-\tilde{\tau}}$ and, hence, the solution to eqn. (21) obey $x < 1/\sqrt{-\tilde{\tau}}$. Further, since

$$\left\{ \begin{array}{rcl} \tau\kappa & > & 1 \\ \tilde{\tau} & = & \tau/(1-\tau\kappa) \end{array} \right. \quad \Rightarrow \quad -\tilde{\tau} > \frac{1}{\kappa},$$

we have $x < \sqrt{\kappa}$. Thus, the singularity $s = x^2 - \kappa$ is located on the negative real axis.

Using $\tanh iy = -i \tan y$, the solutions y_k to eqn. (20) on the imaginary axis are given by:

$$\tilde{\gamma} \tan y = \frac{1}{y} - \tilde{\tau} y. \tag{22}$$

Also the solutions to this equation are centered around the origin. When $\tilde{\tau}$ and $\tilde{\gamma}$ are poisitive the positive solutions to eqn. (22) satisfy

$$0 < y_1 < \frac{\pi}{2} < y_2 < \frac{3\pi}{2} < y_3 < \frac{5\pi}{2} < y_4 < \ \ldots$$

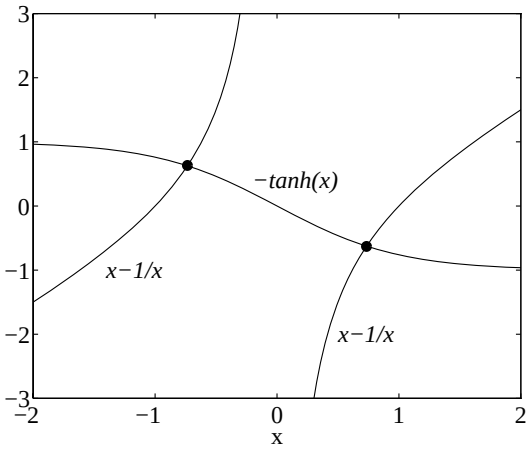

Figure 2: Locations of the solutions $z = x$ when $\tilde{\tau} = -1$ and $\tilde{\gamma} = -1$.

In Figure 3 are the locations of these solutions illustrated for $\tilde{\tau} = 1$ and $\tilde{\gamma} = 1$.

Note that for large $y > 0$, the solutions approximately satisfy

$$\tan y_k = -\infty \quad \Leftrightarrow \quad y_k = -\frac{\pi}{2} + k\pi.$$

When $\tilde{\tau}$ and $\tilde{\gamma}$ are negative the positive solutions satisfy (leaving index 1 for the solution on the real axis)

$$\frac{\pi}{2} < y_2 < \frac{3\pi}{2} < y_2 < \frac{5\pi}{2} < y_4 < \ \ldots$$

In Figure 4 the solutions to eqn. (22) are shown when $\tilde{\tau} = -1$ and $\tilde{\gamma} = -1$.

The solutions y_k on the imaginary axis can readily be found numerically by, e.g., a Newton-Raphson method restricted to the intervals where solutions are of interest.

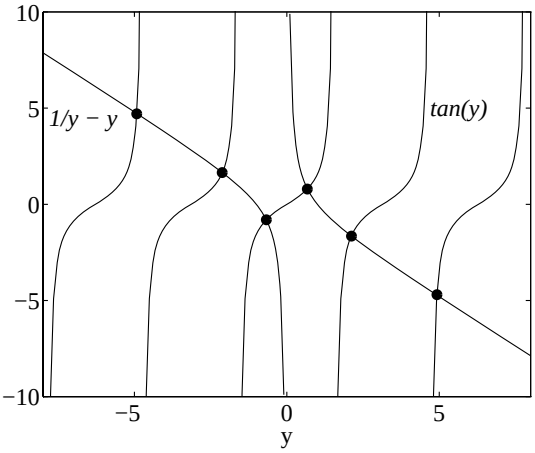

Figure 3: Locations of the solutions $z = iy_k$ when $\tilde{\tau} = 1$ and $\tilde{\gamma} = 1$.

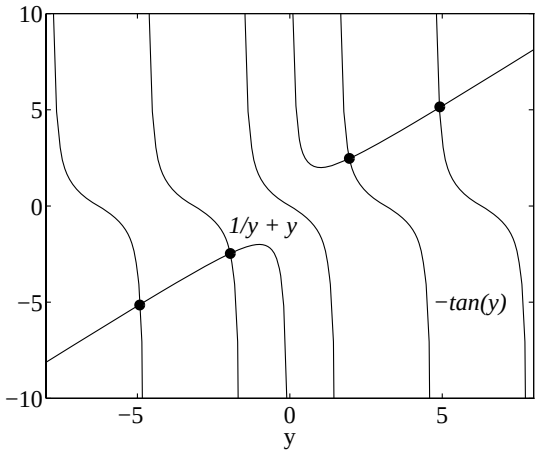

Figure 4: Locations of the solutions $z = iy_k$ when $\tilde{\tau} = -1$ and $\tilde{\gamma} = -1$.

To summarize; when we have no reaction, zero order kinetics, or first order kinetics and $\tau\kappa < 1$, we have one singularity $\alpha_1 = -y_1^2 - \kappa$, where y_1 is a solution to eqn. (22), such that

$$\frac{\pi^2}{4} - \kappa < \alpha_1 < -\kappa.$$

When we have first order kinetics and $\tau\kappa > 1$ there is one negative real singularity $\alpha_1 = x^2 - \kappa$, where x is a solution to eqn. (21). For all kinetics considered, the remaining singularities $\alpha_k = -y_k^2 - \kappa$ are given by eqn. (22), and satisfy

$$-([2k-1]\pi/2)^2 - \kappa < \alpha_k < -([2k-3]\pi/2)^2 - \kappa, \qquad k = 2, 3, \ldots.$$

Since all singularities are located in the left half-plane the transfer function is, not surprisingly, stable for all kinds of kinetics considered.

6 Approximate transfer function

The derived transfer functions (18) and (19) are not suitable for simulation. Instead, approximate transfer functions $\hat{G}_j(s)$ and $\hat{G}(s)$ that are rational functions of polynomials in s are desired. Such transfer functions are suitable for simulations in the time domain, and simple routines are available in many softwares, e.g. MATLAB (control toolbox) and MATRIX-x. Furthermore, such transfer functions can easily be implemented for real time control and simulation.

The key idea is to determine the exact unit impulse response, which equals the inverse Laplace transform, for one CSBR and then find a rational $\hat{G}_j(s)$ that arbitrary well

approximates the exact response. The approximate influent/effluent transfer function $\hat{G}(s)$ then becomes the product of all $\hat{G}_j(s)$. The analysis that follows is based on basic mathematics in complex variables, see e.g. [2].

Denote the denominator of $G_j(s)$ in eqn. (18) by $F(s)$. Then the inverse Laplace transform of $G_j(s)$ is given by

$$g(t) = \lim_{\sigma\to\infty} \frac{1}{2\pi i} \int_{\kappa-i\sigma}^{\kappa+i\sigma} \frac{Ke^{st}}{F(s)} ds.$$

Since the singularities are located left of $s = \kappa$ for both kinds of kinetics, we may use the Residue Theorem to determine the inverse Laplace transform:

$$g(t) = \frac{1}{2\pi i} \oint_{\Omega} \frac{Ke^{st}}{F(s)} ds \tag{23}$$

$$= K \sum_{k=1}^{\infty} \text{Res} \left\{ \frac{e^{st}}{F(s)} \right\}_{s=\alpha_k}, \tag{24}$$

where α_k are the locations of the singularities of $G_j(s)$, and Ω is the region left of $s = \kappa$ in the complex plane.

The denominator $F(s)$ is analytic in a surrounding to each singularity α_k to $G_j(s)$. Hence, there exist a convergent Taylor expansion around each singularity:

$$F(s) = F(\alpha_k) + F'(\alpha_k)(s - \alpha_k) + \sum_{p=2}^{\infty} \frac{F^{(p)}(\alpha_k)}{p!}(s - \alpha_k)^p,$$

where

$$F'(\alpha_k) = \tau + \frac{\gamma}{2\sqrt{\alpha_k}} \left\{ \tanh \sqrt{\alpha_k} + \sqrt{\alpha_k} - \sqrt{\alpha_k} \tanh^2 \sqrt{\alpha_k} \right\}.$$

Since $F'(\alpha_k) \neq 0$ the integrand in eqn. (23) has poles of order one at α_k. The residues can then be determined from

$$\text{Res} \left\{ \frac{e^{st}}{F(s)} \right\}_{s=\alpha_k} = \frac{e^{\alpha_k t}}{F'(\alpha_k)}.$$

Hence, the pulse response becomes

$$g(t) = K \sum_{k=1}^{\infty} \frac{e^{\alpha_k t}}{F'(\alpha_k)}, \tag{25}$$

which is exactly the pulse response of a rational polynomial transfer function

$$\bar{G}(s) = \sum_{k=1}^{\infty} \frac{K}{F'(\alpha_k)(s - \alpha_k)}. \tag{26}$$

Since the singularities rapidly becom largely negative with increasing k, only the first terms in eqn. (25) will be significant, since the others will rapidly approach zero. Hence, an arbitrary well approximation of $G_j(s)$ can be achieved by truncation of the sum in eqn. (26). Truncating the sum after m terms, the approximate transfer function of $G_j(s)$ becomes

$$\hat{G}_j(s) = \frac{K \sum_{l=1}^{m} \prod_{k \neq l} F'(\alpha_k)(s - \alpha_k)}{\prod_{k=1}^{m} F'(\alpha_k)(s - \alpha_k)}, \tag{27}$$

and the approximate transfer function describing the influent/effluent dynamics becomes:

$$\hat{G}(s) = \{\hat{G}_j(s)\}^n. \tag{28}$$

If the reactor is not divided into equal CSBRs, $\hat{G}(s)$ becomes the product of all $\hat{G}_j(s)$.

The approximate transfer function $\hat{G}(s)$ can be compared to the exact transfer function in the frequency domain, e.g. in Bode diagrams, which shows how much a sinusoidal input of frequency ω is gained, i.e. $|G(i\omega)|$, and how many degrees the output sinusoidal is shifted from the input, i.e. $\arg G(i\omega)$. In Figure 5 are $\hat{G}_j$ and G_j compared when $\kappa = 0$, $\tilde{\tau} = 1$ and $\tilde{\gamma} = 1$. Note that the gain is shown in dB ($20 \log_{10} |G(i\omega)|$). The number of singularities considered in eqn. (27) is m=2, and the approximate transfer function, evaluated with eqn. (27), is

$$\hat{G}_j(s) = \frac{1 + 0.4016s}{1.0041 + 2.4198s + 0.4899s^2}$$

As can be seen from the figure, the curves of the approximate transfer function and the curves of the exact transfer function almost coincide in the frequency region considered. The disagreement is in the high frequency region, which corresponds to the fastest dynamic modes. This is natural since it is those modes that have been ignored in the truncation of the exact pulse response. However, the disagreement is hardly of any importance since there is almost no effect of the input on the output due to the low values of the gain at high frequencies. If one additional singularity is included the curves become inseparable in the diagrams, and if only one singularity is considered the curves do not agree at all. In Figure 6 is the Bode diagrams for $\hat{G}$, according to eqn. (28), compared to G when $n = 10$ and $m = 2$. The same observations as for Figure 5 can be made also for this comparison.

6.1 Determination of pulse response

A useful way to acquire information about the fast dynamics in biofilm reactors is to carry out pulse response experiments. Usually, a non-reacting trace substance is added

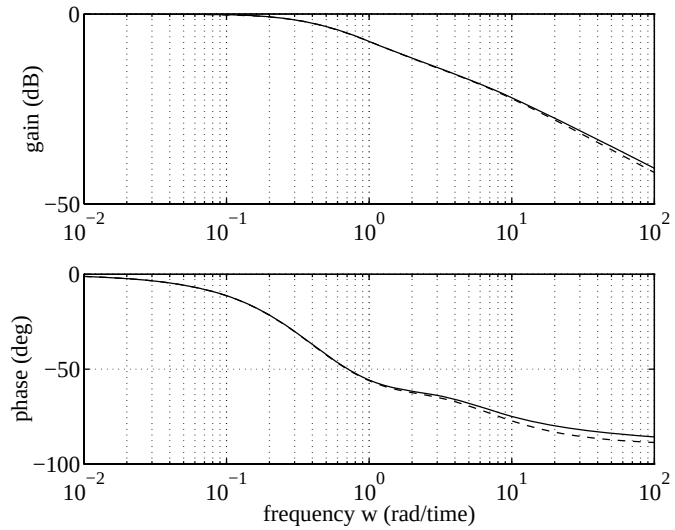

Figure 5: Bode diagram of $G_j(i\omega)$ (solid) and $\hat{G}_j(i\omega)$ (dashed) when $\tilde{\tau} = 1$, $\tilde{\gamma} = 1$, $\kappa = 0$ and $m = 2$.

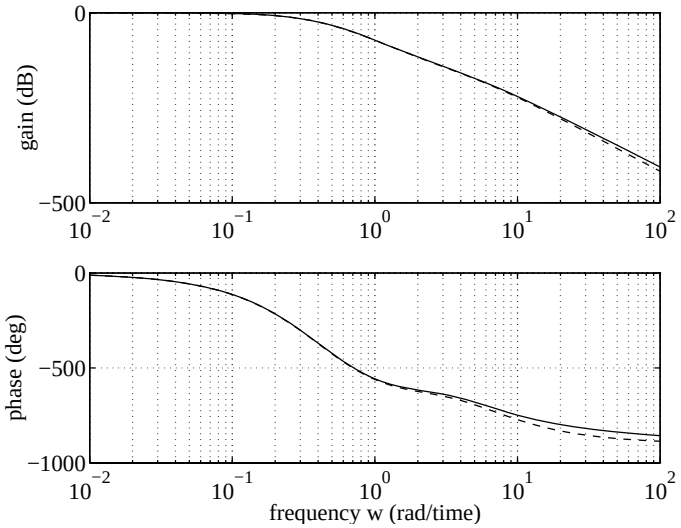

Figure 6: Bode diagram of $G(i\omega)$ (solid) and $\hat{G}(i\omega)$ (dashed) when $\tilde{\tau} = 1$, $\tilde{\gamma} = 1$, $\kappa = 0$, $n = 10$ and $m = 2$.

to the influent and samples are taken from the effluent. Sometimes, however, it may also be possible to achieve pulses in a reacting substrate.

By using the CSBR-model in the analysis of pulse response experiments, important reactor parameters may be possible to determine. Three different methods to calculate pulse responses are presented in this section. The first method is based on the approximate transfer function (27), the second is based on truncation of the exact pulse response of

(19), and the last method is a simple finite difference scheme. All methods are applied to the case of zero order kinetics.

The size of the ideal pulse in the influent has to be determined in terms of the non-dimensional form of the model equations. Let the pulse added to the influent at time $t = 0$ (dimensionless time) be

$$c_0(t) = c_\delta \delta(t), \tag{29}$$

where $\delta(t)$ is the unit Dirac pulse function. By using the scaling of time, i.e. eqn. (5), we have

$$\begin{aligned} \int_{-\infty}^{\infty} Q c_\delta \delta(\bar{t}) d\bar{t} &= Q c_\delta \int_{-\infty}^{\infty} \delta(t) \frac{L^2 \epsilon}{D} dt \\ &= m_\delta, \end{aligned}$$

where m_δ is the additional mass introduced by the pulse in the influent. Hence,

$$c_\delta = \frac{D m_\delta}{Q L^2 \epsilon}.$$

6.1.1 Determination by use of the approximate transfer function

The major uses for the approximate transfer function (28) are in connection with existing software. In many softwares there are ready-to-use routines that simulates the response of an arbitrary input (influent concentration) to any rational polynomial transfer function. However, explicit expressions can found by partial fraction decomposition (PFD) of the approximate transfer function. By carrying out PFD on the products in eqn. (28) we get

$$\hat{G}(s) = K^n \sum_{k=1}^{m} \sum_{j=1}^{n} \frac{b_{kj}}{(s - \alpha_k)^j}. \tag{30}$$

The constants b_{kj} can be determined by, e.g., a recursive algorithm presented in Appendix. From eqns. (29) and (30) the pulse response follows from any table of inverse Laplace transforms:

$$c_n(t) = c_\delta K^n \sum_{k=1}^{m} \sum_{j=1}^{n} \frac{b_{kj} t^{j-1}}{(j-1)!} e^{\alpha_k t}$$

An explicit form of the pulse response may actually be easier to derive if the reactor is not divided into equal CSBRs. If the values of $\tilde{\tau}$ and $\tilde{\gamma}$ are not the same in each CSBR, then the locations α_k of the singularities will also differ. Let α_{kj} be the k :th singularity in the j :th CSBR. Then the approximate transfer function becomes

$$\hat{G}(s) = \prod_{j=1}^{n} \hat{G}_j(s)$$

$$= \prod_{j=1}^{n} \sum_{k=1}^{m} \frac{K}{F'(\alpha_{kj})(s-\alpha_{kj})} \tag{31}$$

$$= K^n \sum_{j=1}^{n} \sum_{k=1}^{m} \frac{b_{kj}}{s-\alpha_{kj}}, \tag{32}$$

where

$$b_{kj} = \frac{1}{F'(\alpha_{kj})} \prod_{\substack{i=1 \\ i \neq j}}^{n} \sum_{l=1}^{m} \frac{1}{F'(\alpha_{li})(\alpha_{kj}-\alpha_{li})} \tag{33}$$

are the constants that result from PFD on the products in (31). The pulse response follows from the inverse Laplace transform of (32):

$$c_n(t) = c_\delta K^n \sum_{j=1}^{n} \sum_{k=1}^{m} b_{kj} e^{\alpha_{kj} t}.$$

As an illustration, consider the case when $m = 2$, $n = 2$, $\kappa = 0$, and $\tau = \gamma = 1$ for one CSBR, and $\tau/2 = \gamma = 1$ for the other CSBR. The approximate transfer function is the product of the two $\hat{G}_j(s)$, evaluated by eqn. (31):

$$\begin{aligned} \hat{G}(s) &= \left(\frac{1}{2.4(s+0.46)} + \frac{1}{2.5(s+4.5)}\right)\left(\frac{1}{3.3(s+0.32)} + \frac{1}{6.8(s+3.5)}\right) \\ &= \frac{0.13}{(s+0.46)(s+0.32)} + \frac{0.061}{(s+0.46)(s+3.5)} + \\ &\quad \frac{0.12}{(s+4.5)(s+0.32)} + \frac{0.06}{(s+4.5)(s+3.5)}. \end{aligned}$$

Partial fraction decomposition according to the "hands on principle", i.e. eqn. (33), gives:

$$\begin{aligned} \hat{G}(s) &= \left(\frac{0.13}{-0.46+0.32} + \frac{0.061}{-0.46+3.5}\right)\frac{1}{s+0.46} + \\ &\quad \left(\frac{0.012}{-4.5+0.32} + \frac{0.06}{-4.5+3.5}\right)\frac{1}{s+4.5} \\ &\quad \left(\frac{0.13}{-0.32+0.46} + \frac{0.12}{-0.32+4.5}\right)\frac{1}{s+0.32} + \\ &\quad \left(\frac{0.061}{-3.5+0.46} + \frac{0.06}{-3.5+4.5}\right)\frac{1}{s+3.5} + \\ &= \frac{-0.93}{s+0.46} - \frac{0.063}{s+4.5} + \frac{0.96}{s+0.32} + \frac{0.04}{s+3.5} \end{aligned}$$

and, hence, the pulse response is

$$c_n(t) = c_\delta(0.96e^{-0.32t} - 0.93e^{-0.46t} + 0.04e^{-3.5t} + 0.063e^{-4.5t}).$$

6.1.2 Truncation of exact response

In the same manner as the Residue theorem was applied to one CSBR, it may be applied to the series of equal CSBRs, to get the impulse response

$$c_n(t) = c_\delta \sum_{k=0}^{m} \text{Res} \left\{ \frac{K^n e^{st}}{F(s)^n} \right\}_{s=\alpha_k} .$$

It can easily be shown that the order of the singularities α_k equals the number of CSBRs in this case, see Appendix.

Then, the following formula for determining the residues may be used:

$$\text{Res} \left\{ \frac{e^{st}}{F(s)^n} \right\}_{s=\alpha_k} = \lim_{s \to \alpha_k} \frac{1}{(n-1)!} \left(\frac{d}{ds} \right)^{n-1} \left[(s-\alpha_k)^n \frac{e^{st}}{F(s)^n} \right]$$

Unfortunately, the terms in eqn. (6.1.2) become quite many and cumbersome as n becomes large. However, if we rewrite eqn. (39) in Appendix as

$$F(s)^n = \sum_{p=0}^{\infty} f_p (s-\alpha_k)^{n+p}$$

the residues become reasonably simple for $n < 5$:

$$\begin{aligned}
\text{Res} \left\{ \frac{e^{st}}{F(s)} \right\}_{s=\alpha_k} &= \frac{e^{\alpha_k t}}{f_0} \\
\text{Res} \left\{ \frac{e^{st}}{F(s)^2} \right\}_{s=\alpha_k} &= \frac{e^{\alpha_k t}}{f_0^2} (f_0 t - f_1) \\
\text{Res} \left\{ \frac{e^{st}}{F(s)^3} \right\}_{s=\alpha_k} &= \frac{e^{\alpha_k t}}{f_0^3} \left(\frac{1}{2} f_0^2 t^2 - f_0 f_1 t + f_1^2 - f_0 f_2 \right) \\
\text{Res} \left\{ \frac{e^{st}}{F(s)^4} \right\}_{s=\alpha_k} &= \frac{e^{\alpha_k t}}{f_0^4} \left(\frac{1}{6} f_0^3 t^3 - \frac{1}{2} f_0^2 f_1 t^2 + (f_0 f_1^2 - f_0^2 f_2) t + (2 f_0 f_1 f_2 - f_0^2 f_3 - f_1^3) \right)
\end{aligned}$$

Note that the coefficients f_k depend on n and α_k. They may either be calculated by the multinomial theorem applied to the Taylor expansion of $F(s)$, by direct Taylor expansion of $F(s)^n$, or from eqn. (38). For the residues above, the coefficients are given in Appendix.

6.1.3 Calculation by finite differences

A completely different approach to determine pulse responses is to attack the original set of differential equations (7) and (8). Since they are linear they may quite easily be solved by, e.g., the method of finite differences. A scheme wil be shown for $\kappa = 0$, but the extension to $\kappa \neq 0$ is straightforward. Discretizing time as $t = k\Delta t, \quad k = 0, 1, \ldots$

and space as $x = l\Delta x, \quad l = 0, 1, \ldots M$, a Crank-Nicholson scheme for eqn. (8), where the subscript j is dropped, is

$$\bar{\partial}_t c_l^{k+1} = \partial_x \bar{\partial}_x \frac{c_l^k + c_l^{k+1}}{2} \quad l = 1, 2, \ldots M-1. \tag{34}$$

Here, ∂_t and $\bar{\partial}_t$ denote the forward and backward difference quotient operator with respect to t:

$$\partial_t c^k = \frac{c^{k+1} - c^k}{\Delta t}, \qquad \bar{\partial}_t c^k = \frac{c^k - c^{k-1}}{\Delta t}.$$

The operators ∂_x and $\bar{\partial}_x$ are equivalently defined.

If we let

$$\lambda = \frac{\Delta t}{\Delta x^2},$$

eqn. (34) can be written as

$$(1+\lambda)c_l^{k+1} - \frac{\lambda}{2}(c_{l+1}^{k+1} + c_{l-1}^{k+1}) = (1-\lambda)c_l^k + \frac{\lambda}{2}(c_{l+1}^k + c_{l-1}^k). \tag{35}$$

The boundary conditions (3) can be introduced as

$$c_1^k = c_0^k \quad \text{and} \quad c_M^k = c_j^{b,k},$$

where $c_j^{b,k}$ is the bulk concentration in the j:th CSBR at time $k\Delta t$. These boundary conditions imply

$$\begin{aligned} (1+\lambda)c_1^{k+1} - \frac{\lambda}{2}c_2^{k+1} &= (1-\lambda)c_1^k + \frac{\lambda}{2}c_2^k \\ (1+\lambda)c_{M-1}^{k+1} - \frac{\lambda}{2}c_{M-2}^{k+1} - \frac{\lambda}{2}c_j^{b,k+1} &= (1-\lambda)c_{M-1}^k + \frac{\lambda}{2}c_{M-2}^k + \frac{\lambda}{2}c_j^{b,k}. \end{aligned}$$

The mass-balance (7) for the bulk concentrations can be discretized as

$$\tau \partial_t c_j^{b,k} = c_{j-1}^{b,k} - c_j^{b,k} - \gamma \bar{\partial}_x c_M^k. \tag{36}$$

By introducing

$$\mu_1 = \frac{\Delta t}{\tau} \quad \text{and} \quad \mu_2 = \frac{\gamma \Delta t}{\tau \Delta x},$$

and using the boundary condition $c_M^k = c_j^{b,k}$, eqn. (36) can be written as

$$c_j^{b,k+1} = \mu_2 c_{M-1}^k + (1 - \mu_1 - \mu_2)c_j^{b,k} + \mu_1 c_{j-1}^{b,k}. \tag{37}$$

The eqns. (35) and (37) for each CST can be written in matrix form as:

$$\begin{bmatrix} 1+\frac{\lambda}{2} & -\frac{\lambda}{2} & 0 & \dots & 0 & 0 \\ -\frac{\lambda}{2} & 1+\lambda & -\frac{\lambda}{2} & & 0 & 0 \\ 0 & -\frac{\lambda}{2} & 1+\lambda & \ddots & 0 & 0 \\ \vdots & & \ddots & \ddots & \ddots & \\ 0 & 0 & \dots & -\frac{\lambda}{2} & 1+\lambda & -\frac{\lambda}{2} \\ 0 & 0 & \dots & 0 & 0 & 1 \end{bmatrix} \begin{bmatrix} c_1^{k+1} \\ c_2^{k+1} \\ \vdots \\ \\ c_{M-1}^{k+1} \\ c_j^{b,k+1} \end{bmatrix} =$$

$$\begin{bmatrix} 1-\frac{\lambda}{2} & \frac{\lambda}{2} & 0 & \dots & 0 & 0 \\ \frac{\lambda}{2} & 1-\lambda & \frac{\lambda}{2} & & 0 & 0 \\ 0 & \frac{\lambda}{2} & 1-\lambda & \ddots & 0 & 0 \\ \vdots & & \ddots & \ddots & \ddots & \\ 0 & 0 & \dots & \frac{\lambda}{2} & 1-\lambda & \frac{\lambda}{2} \\ 0 & 0 & \dots & 0 & \mu_2 & 1-\mu_1-\mu_2 \end{bmatrix} \begin{bmatrix} c_1^k \\ c_2^k \\ \vdots \\ \\ c_{M-1}^k \\ c_j^{b,k} \end{bmatrix} + \begin{bmatrix} 0 \\ 0 \\ \vdots \\ \\ 0 \\ \mu_2 \end{bmatrix} c_{j-1}^{b,k}$$

which more compactly is written as

$$\Lambda_1 C_j^{k+1} = \Lambda_2 C_j^k + \Lambda_3 c_{j-1}^{b,k}, \quad j = 1, 2, \dots n.$$

Thus, a recursive form for the effluent concentration from each CSBR is

$$\begin{aligned} C_j^{k+1} &= \Lambda_1^{-1}\Lambda_2 C_j^k + \Lambda_1^{-1}\Lambda_3 c_{j-1}^{b,k}, \quad j = 1, 2, \dots n \\ c_j^{k+1} &= C_j^{k+1}(M+1) \end{aligned}$$

Stability of the method is ensured if the eigenvalues of $\Lambda_1^{-1}\Lambda_2$ are within the unit circle, and a discretization with approximately $M = 100$ is required for reasonable accuracy. The method can be used to simulate arbitrary influent concentrations $c_0^{b,k}$. For the simulation of pulse responses, the influent concentration is

$$c_0^{b,k} = \begin{cases} c_\delta/\Delta t & : \quad k = 0 \\ 0 & : \quad k = 1, 2, \dots \end{cases}$$

and the remaining initial values are zero.

A general problem with schemes of this kind is associated with the inversion of Λ_1. As the discretization is made finer (large M) for better accuracy, the condition number for Λ_1 becomes vary large. The large condition number means that the matrix is close to singular, which gives deteriorating numerical accuracy in the inversion. To avoid such problems, a numerically sound method for the inversion is required. In this study, the inversions are carried out using the singular value decomposition of Λ_1.

7 Simulations

7.1 Pulse responses

Comparison between the methods

In this section the methods presented for determining pulse responses are compared. The largest number of CSBRs that an explicit expression has been derived for the exact response (see Appendix) is $n = 4$. This number of CSBRs, $\kappa = 0$ (zero order dynamics or no reaction), $\tau = 1$ and $\gamma = 1$ are used in the comparisons. Simulations using the approximate transfer function are carried out both with the ready-to-use MATLAB-routines *impulse* and *lsim*, which only requires the numerator and denominator polynomials of $\hat{G}(s)$, and by using the PFD-algorithm in Appendix.

In Figure 7, the response is shown as determined by truncation of the exact response when $m = 20$ and $n = 4$. Considering this response as the exact response, we can determine the errors of different approximations. In Table 1 are the comparisons summarized. The maximum error, the dimensionless time when it occurs, the normed error, and the number of arithmetic operations (*flops*) are given. The normed error, corresponding to a mean standard deviation, is defined as

$$||e|| = \left(\frac{1}{30} \int_0^{30} e^2(t) dt \right)^{0.5},$$

where the error $e(t)$ is the difference to the truncated exact response ($m = 20$). The time difference between each evaluation of the responses was $\Delta t = 0.01$ for all methods.

As can be seen from Table 1 the method of exact truncation is the most accurate and most efficient method. Already a truncation after two singularities gives ignorable errors. The method of finite differences requires a fine discretization to give acceptable results, which results in a large number of operations. It should be noted, however, that the number of operations may most likely be reduced for all methods if the routines used are numerically optimized.

Dependency on parameters

Often, reactors, such as trickling filters, does not have a natural division into an exact number of CSBRs. A model with cascaded CSBRs is rather a tool for describing the hydraulics and dynamics. Considering the volume V and the area of biofilm A as fixed,

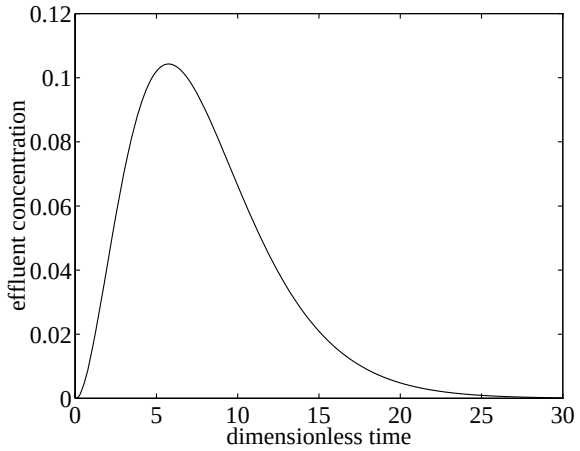

Figure 7: Unit impulse response for $n = 4$, $\kappa = 0$, $\tau = 1$ and $\gamma = 1$.

Table 1: Comparison of unit pulse responses

Method		$\max\|e(t)\|$	t_{max}	$\|\|e\|\|$	# operations
Exact truncation	$m = 2$	$1.2 \cdot 10^{-5}$	0	$2.8 \cdot 10^{-7}$	$0.18 \cdot 10^{6}$
Exact truncation	$m = 3$	$4.2 \cdot 10^{-7}$	0	$6.9 \cdot 10^{-9}$	$0.27 \cdot 10^{6}$
Approx. (MATLAB)	$m = 2$	$2.1 \cdot 10^{-3}$	3.79	$8.9 \cdot 10^{-4}$	$0.50 \cdot 10^{6}$
Approx. (MATLAB)	$m = 3$	$3.6 \cdot 10^{-4}$	3.74	$1.6 \cdot 10^{-4}$	$0.79 \cdot 10^{6}$
Approx. (MATLAB)	$m = 4$	$1.1 \cdot 10^{-4}$	3.72	$4.9 \cdot 10^{-5}$	$1.14 \cdot 10^{6}$
Approx. (PFD)	$m = 2$	$2.1 \cdot 10^{-3}$	3.79	$8.9 \cdot 10^{-4}$	$0.12 \cdot 10^{6}$
Approx. (PFD)	$m = 3$	$3.7 \cdot 10^{-4}$	3.75	$1.6 \cdot 10^{-4}$	$0.15 \cdot 10^{6}$
Approx. (PFD)	$m = 4$	$1.2 \cdot 10^{-4}$	3.74	$5.1 \cdot 10^{-5}$	$0.19 \cdot 10^{6}$
Approx. (PFD)	$m = 10$	$4.7 \cdot 10^{-6}$	3.74	$2.0 \cdot 10^{-6}$	$0.40 \cdot 10^{6}$
Finite differences	$M = 10$	$8.9 \cdot 10^{-3}$	3.65	$3.7 \cdot 10^{-3}$	$2.68 \cdot 10^{6}$
Finite differences	$M = 50$	$2.4 \cdot 10^{-3}$	3.18	$9.8 \cdot 10^{-4}$	$64.3 \cdot 10^{6}$
Finite differences	$M = 100$	$1.7 \cdot 10^{-3}$	2.84	$6.7 \cdot 10^{-4}$	$266 \cdot 10^{6}$

how does the division affect the pulse response? In Figure 8, unit impulse responses are shown for increasing numbers of CSBRs in the case of zero order reaction (or no reaction).

For som biofilm reactors, e.g. rotating biological contactors, each CSBR may actually reflect a physical reactor compartment. When designing an extension of such a reactor it may be of interest to know how the dynamics is affected. Mathematically, the values of τ and γ will then remain constant, while n increases. This is illustrated in Figure 9.

In the following simulations are $n = 4$ and the remaining parameters are chosen to give

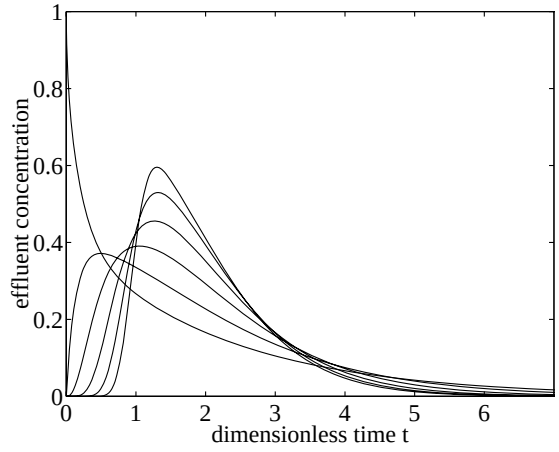

Figure 8: Unit impulse responses when $\kappa = 0$, $\tau = 1/n$ and $\gamma = 1/n$, $n = 1, 2, 4, 8, 16$ and 32 (counted from the left).

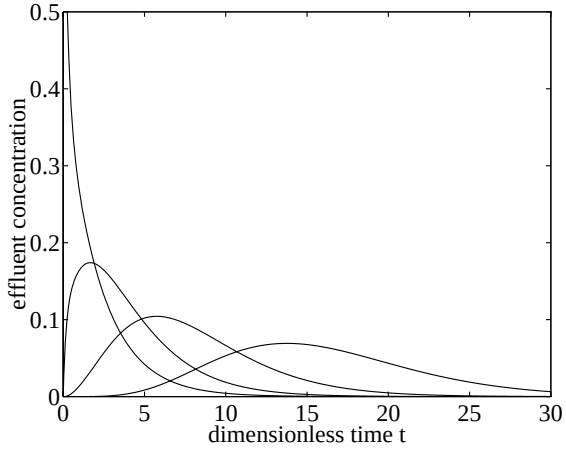

Figure 9: Unit impulse responses when $\kappa = 0$, $\tau = 1$, $\gamma = 1$ and $n = 1, 2, 4$ and 8 (counted from the left).

$\tau = 1/4$ and $\gamma = 1/4$ as standard setting. The dependency on the studied parameters are studied by setting them to a multiple of their standard value, which is denoted by 1. For instance, 2 denotes twice the standard value and 0.6 denotes a 40% reduction of the standard value.

The effects of changes in ϵ and D are shown in Figure 10 for the case of zero order kinetics (or no reaction). Obviously, a change in biofilm water content affects the response far more than a change in the diffusion coefficient. As can also be seen, a larger fraction of water content (ϵ) in the biofilm gives a flatter and slower response, and a larger diffusion coefficient (D) gives a slower response. Both these observations can be attributed to an

increased withhold of substance in the biofilm.

The effects of changes in biofilm thickness (L) and bulk water flow (Q) are shown in Figure 11 for the case of zero order kinetics (or no reaction). A thicker biofilm gives flatter and slower response, which also can be attributed to an increased withhold of substance in the biofilm. Further, a higher flow gives, naturally, a faster response. Note the differences in shape of the responses compared with those in Figure 10. Mainly the tails of the responses are affected by an increase in biofilm thickness, while also the peaks of the responses are changed by an increase in the fraction of biofilm water content.

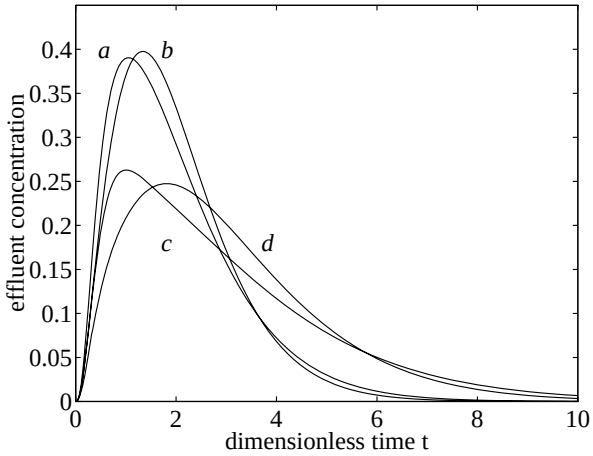

Figure 10: Pulse responses when $\kappa = 0$ and; $D = 1$, $\epsilon = 1$ (a), $D = 2$, $\epsilon = 1$ (b), $D = 1$, $\epsilon = 2$ (c), and $D = 2$, $\epsilon = 2$ (d).

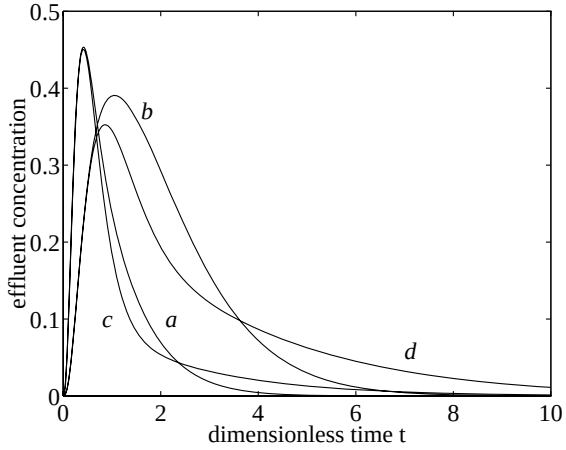

Figure 11: Pulse responses when $\kappa = 0$ and; $L = 1$, $Q = 2$ (a), $L = 1$, $Q = 1$ (b), $L = 2$, $Q = 2$ (c), and $L = 2$, $Q = 1$ (d).

The effects of the biofilm diffusion is obviously dependent on the biofilm (water) volume compared to that of the bulk (V). The biofilm water volume equals $AL\epsilon$. Hence, the remaining parameter that affects this relation is the biofilm area (A). No area of biofilm gives a model with only cascaded continuously stirred tanks (CSTs). In Figure 12 are the responses shown for zero order kinetics and increasing biofilm area. As expected, an increase in biofilm area gives flatter and slower response.

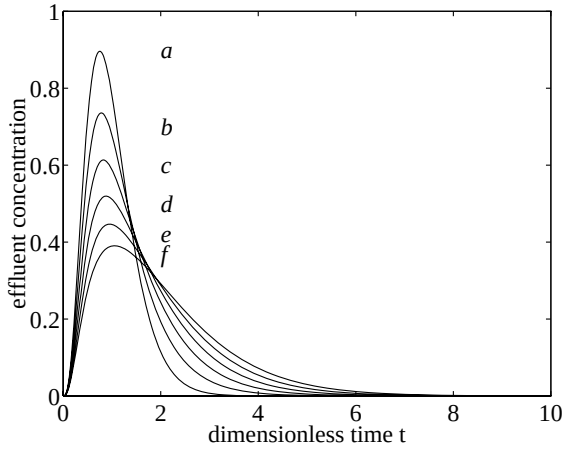

Figure 12: Pulse responses when $\kappa = 0$ and; $A = 0$ (a), $A = 0.2$ (b), $A = 0.4$ (c), $A = 0.6$ (d), $A = 0.8$ (e), and $A = 1.0$ (f).

Finally, the effects of the kinetic constants should be studied for the case of first order kinetics. Typical values of κ ranges from zero to about 100. In Figure 13 pulse responses are shown for values of κ in this interval. As can be seen from the figure, the height of the pulses are very dependent on κ, particularly when κ is small.

Parameter identification

Trace substance pulse response experiments can be valuable for parameter identification. For example, standard procedures are used for determining bulk water volume and number of tanks in models of cascaded CSTs, using theory and pulse response experiments [3]. These parameters can naturally also be determined for cascaded CSBRs, using the CSBR-model and the derived transfer functions.

The approximate transfer function enables fast simulations for arbitrary n, and hence least square algorithms may easily be used for identification of reactor parameters. As an illustration are used experimental data from five trace substance pulse response experiments, carried out on a pilot plant at Rya WWTP in Göteborg [10]. The experiments

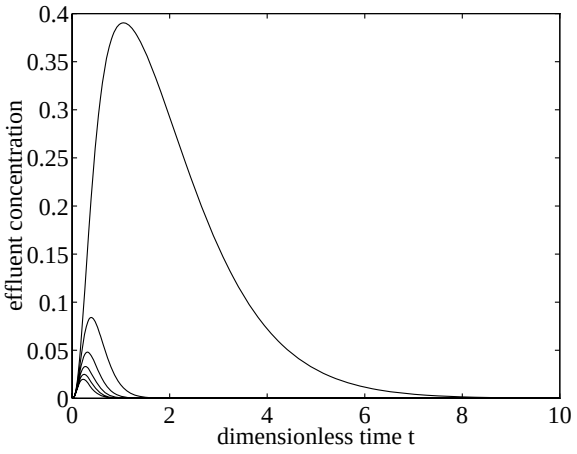

Figure 13: Pulse responses when $n = 4$, $\tau = 1/4$, $\gamma = 1/4$, and $\kappa = 0$, 20, 40, 60, 80 and 100 (ordered from top to bottom).

were carried out at two different flows: 7.3 l/s (two experiments) and 14.5 l/s (three experiments). A description of the pilot plant and the experimental setup can be found in [9, 10].

The parameters that are identified are the total volume V and an appropriate number n of CSBRs. The remaining parameters are: $D_{Li} = 0.4 \cdot 10^{-5}$ m^{2}d^{-1}, $L = 0.5$ mm, $\epsilon = 0.3$, and $A = 9320$ m^2. The values used for the biofilm thickness and fraction of water content in the biofilm are values that have been roughly estimated visually and used in earlier simulations [9, 10, 8]. A least square fitting of data to responses simulated with the approximate transfer function resulted in $n = 9$ and $V = 2.70$ m^3 at $Q = 7.3$ l/s, respectively $n = 8$ and $V = 3.47$ m^3 at $Q = 14.5$ l/s. The corresponding simulated and measured responses are shown in Figures 14 and 15.

As can be seen from the figures, the agreement between simulated and measured data is very good. However, the simulated tail in Figure 14, which declines too fast, indicates that a larger value for the biofilm thickness may improve the agreement. A least square identification of n, V and also L at $Q = 7.3$ l/s gives $n = 10$, $V = 2.59$ m^3 and $L = 0.571$ mm, and, hence, a thicker biofilm as expected. Due to too noisy data when $Q = 14.5$ l/s a similar least square identification fails, but using the same thickness as for $Q = 7.3$ in an identification of n and V gives $n = 9$, $V = 3.41$, and reduces the sum of squares by 11%. These simulations are included in Figures 14 and 15.

From Figures 10 and 11 it is evident that the diffusion coefficient and the flow changes the pulse responses differently at different values of the biofilm thickness and fraction of water content. Thus, the use of different trace substances in pulse response experiments carried

out at different flows can become useful when identifying the efficient biofilm thickness and water content, as well as bulk water volume and an appropriate number of CSBRs.

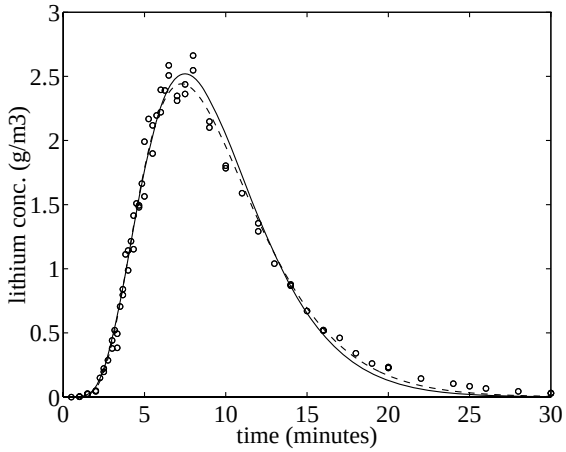

Figure 14: Measured pulse responses at $Q = 7.3$ l/s, and simulated response when $n = 9$, $V = 2.70$ m^3, $L = 0.5$ mm (solid), and $n = 10$, $V = 2.59$ m^3, $L = 0.571$ mm (dashed).

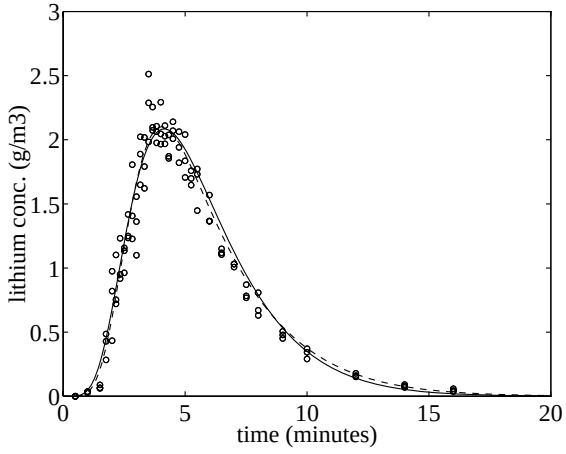

Figure 15: Measured pulse responses at $Q = 14.5$ l/s, and simulated response when $n = 8$, $V = 3.47$ m^3, $L = 0.5$ mm (solid), and $n = 9$, $V = 3.41$ m^3, $L = 0.571$ mm (dashed).

7.2 Step responses

Step responses may either be determined by integration of pulse responses or numerically by using the approximate transfer function. Here, we will only show numerically simulated step responses when the number of CSBRs are increased while V and A remain the same (Figure 16) at zero order kinetics, and when $n = 4$ and κ is increased for the case of first

order kinetics (Figure 17). Note that the effluent concentrations in the figures denotes changes in effluent concentration from initial stationary values. An interesting feature for the case of first order kinetics is that the dynamics become faster as κ increases.

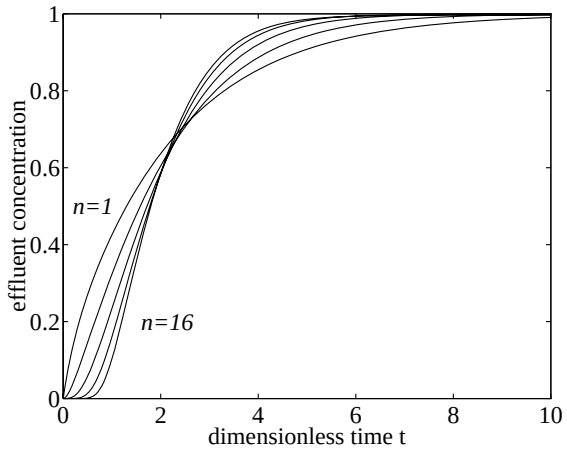

Figure 16: Step responses when $\kappa = 0$, $\tau = 1/n$, $\gamma = 1/n$, and $n = 1$, 2, 4, 8 and 16 (ordered from the lower left).

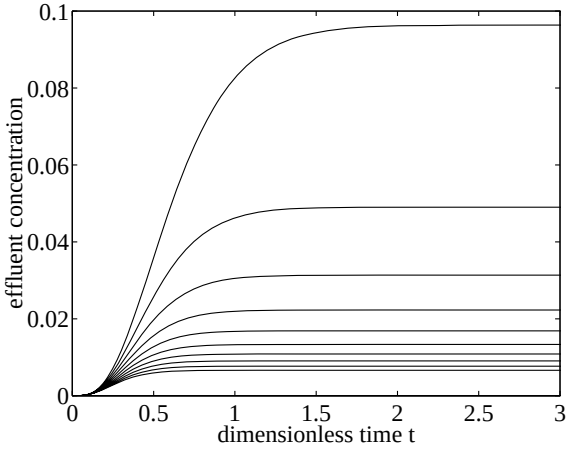

Figure 17: Step responses when $n = 4$, $\tau = 1/4$, $\gamma = 1/4$, and $\kappa = 10$, 20, 30, ... 100 (ordered from top to bottom).

8 Conclusion and discussion

A fairly simple model describing the fast dynamics of cascaded continuously stirred biofilm reactors (CSBRs) has been formulated. The model includes flexibilities, such as independent biofilm thickness, bulk water volume, biofilm water content, diffusion characteristics,

kinetics, bacterial concentration (which may depend on depth in the biofilm) and biofilm area, in each CSBR. If zero or first order kinetics is used for the reaction in the biofilm, the model is linear, and an analytical transfer function can be determined. From the exact transfer function, which is unsuitable for simulations, can an approximate transfer function be determined. With the approximate transfer function, simulations of arbitrary influent concentrations can be carried out at a low cost of computation.

The model equations may also be solved by simple finite difference schemes. Such schemes are easy to make and use, but have several disadvantages compared to the transfer function approach. The transfer function approach is numerically much more efficient and accurate, and it may also be used for studies in the frequency domain, which is important for controller design. Due to the numerical efficiency, the exact and approximate transfer function are suitable for the determination of pulse responses, and parameter identification using, e.g., least squares.

Trace substance pulse response data from a pilot scale trickling filter show very good agreement with model simulations, and it was possible to estimate the bulk water volume, an appropriate number of CSBRs, and biofilm thickness from experimental data.

References

[1] J. J. DiStefano, A. R. Stebberud, and I. J. Williams. *Theory and problems of feedback and control systems.* Schaum's outline series. McGraw-Hill Inc., New York, USA., 1967. p. 58.

[2] S. D. Fischer. *Complex variables.* Mathematics series. Wadsworth & Brooks/Cole, Pacific Grove, California 93950, USA, 2nd edition, 1990.

[3] G. F. Froment and K. B. Bischoff. *Chemical Reactor Analysis & Design.* Wiley, New York, 1979.

[4] W. Gujer and M. Boller. Design of a nitrifying tertiary trickling filter based on theoretical concepts. *Wat. Res.*, 20(11):1353–1362, 1986.

[5] G. Strang. *Linear algebra and its applications.* Harcourt Brace Jovanovich, Inc., Orlando, Florida 32887, USA, 3rd edition, 1988.

[6] D. V. Vayenas and G. Lyberatos. A novel model for nitrifying trickling filters. *Wat. Res.*, 28(6):1275–1284, 1994.

[7] O. Wanner and W. Gujer. Competition in biofilms. *Wat. Sci. Tech.*, 17:27–44, 1984.

[8] T. Wik and C. Breitholtz. Steady-state solution of a two-species biofilm problem. *Biotech. Bioeng.*, 50(6):675–686, 1996.

[9] T. Wik and C. Lindeborg. Modelling the dynamics of a trickling filter for waste water treatment. In *The Third IEEE Conf. on Control Appl.*, pages 1035–1040, Glasgow, UK, August 24th-26th 1994. The IEEE Control Systems Society, New York.

[10] T. Wik, A. Mattsson, E. Hansson, and C. Niklasson. Nitrification in a tertiary trickling filter at high hydraulic loads. *Wat. Sci. Tech.*, 32(8):185–192, 1995.

Appendix

Simulation of an arbitrary influent concentration

The response to any changes in influent concentration can be determined by first converting the approximate transfer function to a state-space form, and then use an integration method. The method presented applies to the case when the division of the reactor is made into equal CSBRs, as well as when they are not equal. Denoting the k:th singularity of the j:th CSBR by α_{kj}, the effluent concentration from the j:th CSBR is related to the influent by

$$C_j^b(s) = \left(\sum_{k=1}^{m} \frac{1}{F'(\alpha_{kj})(s - \alpha_{kj})} \right) C_{j-1}^b(s)$$

By Laplace transforming the following equation, it is easy to verify that the corresponding relation in the time-domain is

$$\begin{aligned} \frac{d}{dt} w_j(t) &= \begin{bmatrix} \alpha_{1j} & 0 & \cdots & 0 \\ 0 & \alpha_{2j} & \cdots & 0 \\ \vdots & & \ddots & \vdots \\ 0 & \cdots & 0 & \alpha_{mj} \end{bmatrix} w_j(t) + \begin{bmatrix} 1 \\ 1 \\ \vdots \\ 1 \end{bmatrix} c_{j-1}^b(t) \\ c_j^b(t) &= \begin{bmatrix} \frac{1}{F'(\alpha_{1j})} & \frac{1}{F'(\alpha_{2j})} & \cdots & \frac{1}{F'(\alpha_{mj})} \end{bmatrix} w_j(t), \end{aligned}$$

where $w_j(t)$ is a column vector with m state variables. We may write this more compactly as

$$\begin{aligned} \frac{d}{dt} w_j(t) &= A_j w_j(t) + B c_{j-1}(t) \\ y(t) &= D_j w_j(t), \end{aligned}$$

where A_j is the m by m matrix with the singularities of the j:th CSBR as diagonal entries, B is the m by 1 vector with unit entries, and D_j is the 1 by m vector with the inverses of the numerator derivatives at the singularities. Using this notation we may write a state-space representation for the entire reactor as:

$$\frac{d}{dt} \begin{bmatrix} w_1(t) \\ w_2(t) \\ \vdots \\ \vdots \\ w_n(t) \end{bmatrix} = \begin{bmatrix} A_1 & 0 & 0 & \cdots & 0 \\ BD_1 & A_2 & 0 & \cdots & 0 \\ 0 & BD_2 & A_3 & & 0 \\ \vdots & & & \ddots & 0 \\ 0 & 0 & \cdots & BD_n & A_n \end{bmatrix} \begin{bmatrix} w_1(t) \\ w_2(t) \\ \vdots \\ \vdots \\ w_n(t) \end{bmatrix} + \begin{bmatrix} B \\ 0 \\ \vdots \\ \vdots \\ 0 \end{bmatrix} c_0^b(t)$$

$$\begin{bmatrix} c_1^b(t) \\ c_2^b(t) \\ \vdots \\ c_n^b(t) \end{bmatrix} = \begin{bmatrix} D_1 & 0 & \cdots & 0 \\ 0 & D_2 & & 0 \\ \vdots & & \ddots & \vdots \\ 0 & 0 & \cdots & D_n \end{bmatrix} \begin{bmatrix} w_1(t) \\ w_2(t) \\ \vdots \\ w_n(t) \end{bmatrix}$$

This equation may numerically be solved with almost any integration method. Note that the original n partial differential equations describing the concentrations in the biofilm, and the n ordinary differential equations describing the concentrations in the bulk water, have been approximated by a linear set of nm ordinary differential equations. Since $m = 2$ in many cases gives a good approximation with the same number of equations, it is unlikely that there exists a reasonable approximation with less equations. Specifically, note that this method requires $n(M+1) - nm$ equations less than, e.g. the presented method of finite differences. Furthermore, arbitrary well approximations can be achieved by increasing the number m of singularities, independently of the integration method used. Thus, it does not suffer from the refinement problem discussed for the method of finite differences.

Order of the singularities of $G(s)$

Since $F(\alpha_k) = 0$ we have

$$\begin{aligned} F(s)^n &= [F'(\alpha_k)(s-\alpha_k) + \sum_{p=2}^{\infty} \frac{F^{(n)}(\alpha_k)}{p!}(s-\alpha_k)^p]^n \\ &= F'(\alpha_k)^n (s-\alpha_k)^n + \\ &\quad \sum_{k=1}^{n} \binom{n}{k} \{F'(\alpha_k)(s-\alpha_k)\}^{n-k} \left\{ \sum_{j=2}^{\infty} \frac{F^{(n)}(\alpha_k)}{j!}(s-\alpha_k)^j \right\}^k \qquad (38) \\ &= (s-\alpha_k)^n (F'(\alpha_k)^n + \mathcal{O}[(s-\alpha_k)]). \qquad (39) \end{aligned}$$

Further, since $F(s)$ is analytic in a surrounding to α_k and the product of analytic functions always are analytic, $\mathcal{O}[(s-\alpha_k)]$ denotes a convergent sum of powers of $(s-\alpha_k)$. Hence, α_k is a pole of order n to $e^{st}/F(s)^n$ since $F'(\alpha_k) \neq 0$ and

$$\begin{aligned} \frac{e^{st}}{F(s)^n} &= (s-\alpha_k)^{-n} \frac{e^{st}}{F'(\alpha_k)^n + \mathcal{O}[(s-\alpha_k)]} \\ &= (s-\alpha_k)^{-n} h(s), \end{aligned}$$

where $h(s)$ is a non-zero analytic function in the neighborhood of α_k.

Taylor coefficients

In Table 2 below are the Taylor coefficients $d_j = F^{(j)}(\alpha_k)/j!$ for an expansion around the singularities α_k given.

Table 2: Taylor coefficients for $F(s)^n$

n	f_0	f_1	f_2	f_3
1	d_1	–	–	–
2	d_1^2	$2d_1d_2$	–	–
3	d_1^3	$3d_1^2d_2$	$3(d_1^2d_3 + d_1d_2^2)$	–
4	d_1^4	$4d_1^3d_2$	$4d_1^3d_3 + 6d_1^2d_2^2$	$4(d_1d_2^3 + 3d_1^2d_2d_3 + d_1^3d_4)$

In the case of negative $\tilde{\tau}$ and $\tilde{\gamma}$ it is easy to show, by straightforward differentiation and insertion of $\sqrt{\alpha_1} = x$, that the coefficients are

$$
\begin{aligned}
d_1 &= \tilde{\tau} + \frac{\tilde{\gamma}}{2x}\left\{\tanh x + x - x\tanh^2 x\right\} \\
d_2 &= \frac{\tilde{\gamma}}{8x^3}\left\{2x^2\tanh^3 x - x\tanh^2 x - (1+2x^2)\tanh x + x\right\} \\
d_3 &= \frac{\tilde{\gamma}}{48x^5}\left\{-6\,x^3\tanh^4 x + (3x+8x^3)\tanh^2 x + 3\tanh x - 3x - 2x^3\right\} \\
d_4 &= \frac{\tilde{\gamma}}{384x^7}\left\{24x^4\tanh^5 x + 12x^3\tanh^4 x - (40x^4+6x^2)\tanh^3 x - (15x+16x^3)\tanh^2 x + \right. \\
&\quad \left. (6x^2 - 15 + 16x^4)\tanh x + 4x^3 + 15x\right\}
\end{aligned}
$$

By insertion of $\sqrt{\alpha_k} = iy_k$, the remaining coefficients, or all coefficients when $\tilde{\tau}$ and $\tilde{\gamma}$ are positive, become

$$
\begin{aligned}
d_1 &= \tilde{\tau} + \frac{\tilde{\gamma}}{2y_k}\left\{y_k + \tan y_k + y_k\tan^2 y_k\right\} \\
d_2 &= \frac{\tilde{\gamma}}{8y_k^3}\left\{-y_k + (1-2y_k^2)\tan y_k - y_k\tan^2 y_k - 2y_k^2\tan^3 y_k\right\} \\
d_3 &= \frac{\tilde{\gamma}}{48y_k^5}\left\{2y_k^3 - 3y_k + 3\tan y_k + (8y_k^3 - 3y_k)\tan^2 y_k + 6y_k^3\tan^4 y_k\right\} \\
d_4 &= \frac{\tilde{\gamma}}{384y^7}\left\{4y_k^3 - 15y_k + (15 + 6y_k^2 - 16y_k^4)\tan y_k + (16y_k^3 - 15y_k)\tan^2 y_k + \right. \\
&\quad \left. (6y_k^2 - 40y_k^4)\tan^3 y_k + 12y_k^3\tan^4 y_k - 24y_k^4\tan^5 y_k\right\}
\end{aligned}
$$

Partial Fraction Decomposition

The coefficients b_{kj} in eqn. (30), which result from partial fraction decomposition of the influent/effluent approximate transfer function, are to be determined. There are several possibilities to calculate those. Two such methods are presented: A recursive formula in the number n of CSBRs, and a set of linear equations to solve. However, for the recursive formula we first need a useful identity:

Lemma 1 *If $\alpha_k \neq \alpha_p$ the following identity holds for all s, and integers r:*

$$\frac{1}{(s-\alpha_k)^r(s-\alpha_p)} = \sum_{q=1}^{r} \frac{(-1)^{r-q}}{(\alpha_k-\alpha_p)^{r-q+1}(s-\alpha_k)^q} + \frac{1}{(\alpha_p-\alpha_k)^r(s-\alpha_p)} \tag{40}$$

Proof From the law of partial fraction decomposition there exist unique constants A_q and B such that

$$\frac{1}{(s-\alpha_k)^r(s-\alpha_p)} = \sum_{q=1}^{r} \frac{A_q}{(s-\alpha_k)^q} + \frac{B}{s-\alpha_p} \tag{41}$$

If we multiply eqn. (41) by $(s-\alpha_p)$ and let $s=\alpha_p$ we get

$$B = \frac{1}{(\alpha_p-\alpha_k)^r}.$$

Multiplication of eqn. (41) by $(s-\alpha_k)^r$ gives

$$\frac{1}{s-\alpha_p} = \sum_{q=1}^{r} A_q(s-\alpha_k)^{r-q} + B\frac{(s-\alpha_k)^r}{s-\alpha_p}.$$

Repeated differentiation $p = 0, 1, \ldots$ times gives

$$\begin{aligned} \frac{d^p}{ds^p}\left(\frac{1}{s-\alpha_p}\right) &= \frac{p!(-1)^p}{(s-\alpha_p)^{p+1}} \\ &= \sum_{q=1}^{r-p} A_q \frac{(r-q)!}{(r-q-p)!}(s-\alpha_k)^{r-q-p} + B\frac{d^p}{ds^p}\left(\frac{(s-\alpha_k)^r}{s-\alpha_p}\right). \end{aligned} \tag{42}$$

By successive differentiation it is readily verified that

$$\frac{d^p}{ds^p}\left(\frac{(s-\alpha_k)^r}{s-\alpha_p}\right) = \frac{r!}{(r-p)!}\frac{(s-\alpha_k)^{r-p}}{s-\alpha_p} + \mathcal{O}[(s-\alpha_k)^{r-p+1}],$$

where $\mathcal{O}[(s-\alpha_k)^{r-p+1}]$ denotes a function were all terms are powers of at least $(s-\alpha_k)^{r-p+1}$. Thus, the last term in eqn. (42) goes to zero as $s \to \alpha_k$ for all $p < r$. This implies that by letting $s = \alpha_k$ in eqn. (42) we get

$$\frac{p!(-1)^p}{(\alpha_k-\alpha_p)^{p+1}} = A_{r-p}p!, \quad p = 0, 1, \ldots r-1$$

and, hence, by a change of variable $q = r - p$

$$A_q = \frac{(-1)^{r-q}}{(\alpha_k - \alpha_p)^{r-q+1}}, \quad q = 1, 2, \ldots r.$$

Insertion of the coefficients A_q and B into eqn. (41) gives the proposed expression (40).

■

The following lemma gives recursive equations for the determination of the coefficients resulting from PFD of the approximate transfer function.

Lemma 2 *If the coefficients in eqn. (30) for n cascaded CSBRs are denoted $b_{kj,n}$ they may be determined recursively ($l = 2, 3 \ldots n$) by*

$$b_{k1,1} = 1/F'(\alpha_k) \tag{43}$$

$$b_{kj,l} = \begin{cases} \displaystyle\sum_{r=1}^{l-1} \sum_{\substack{p=1 \\ p \neq k}}^{m} \frac{b_{pr,(l-1)} b_{k1,1} - (-1)^r b_{kr,(l-1)} b_{p1,1}}{(\alpha_k - \alpha_p)^r} & ; \quad j = 1 \\ b_{k(j-1),(l-1)} b_{k1,1} + \displaystyle\sum_{r=j}^{l-1} \sum_{\substack{p=1 \\ p \neq k}}^{m} \frac{(-1)^{r-j} b_{kr,(l-1)} b_{p1,1}}{(\alpha_k - \alpha_p)^{r-j+1}} & ; \quad j = 2, 3 \ldots l-1 \\ b_{k(l-1),(l-1)} b_{k1,1} & ; \quad j = l \end{cases} \tag{44}$$

where the middle term in eqn. (44) should only be used for $l > 2$.

Proof According to the laws of partial fraction decomposition, there exist unique constants $b_{kj,n}$ in eqn. (30) for all n. The coefficients $b_{k1,1}$ follows directly from the definition of the approximate transfer function for one single CSBR. Using eqn. (30) for the transfer function for $l - 1$ cascaded CSBRs, the transfer function for l cascaded CSBRs can be written as the product of that transfer function with the one for a single CSBR:

$$\begin{aligned} \hat{G}(s) &= \left(\sum_{k=1}^{m} \sum_{r=1}^{l-1} \frac{b_{kr,(l-1)}}{(s - \alpha_k)^r} \right) \left(\sum_{p=1}^{m} \frac{b_{p1,1}}{s - \alpha_p} \right) \\ &= \sum_{r=1}^{l-1} \sum_{k=1}^{m} \sum_{p=1}^{m} \frac{b_{kr,(l-1)} b_{p1,1}}{(s - \alpha_k)^r (s - \alpha_p)} \\ &= \sum_{r=1}^{l-1} \sum_{k=1}^{m} \left(\frac{b_{kr,(l-1)} b_{k1,1}}{(s - \alpha_k)^{r+1}} + \sum_{p \neq k}^{m} \frac{b_{kr,(l-1)} b_{p1,1}}{(s - \alpha_k)^r (s - \alpha_p)} \right). \end{aligned}$$

Using Lemma 1 we have

$$\begin{aligned} \hat{G}(s) &= \sum_{r=1}^{l-1} \sum_{k=1}^{m} \frac{b_{kr,(l-1)} b_{k1,1}}{(s - \alpha_k)^{r+1}} + \\ &\quad \sum_{r=1}^{l-1} \sum_{k=1}^{m} \sum_{p \neq k}^{m} \left(\sum_{q=1}^{r} \frac{(-1)^{r-q} b_{kr,(l-1)} b_{p1,1}}{(\alpha_k - \alpha_p)^{r-q+1} (s - \alpha_k)^q} + \frac{b_{kr,(l-1)} b_{p1,1}}{(\alpha_p - \alpha_k)^r (s - \alpha_p)} \right). \end{aligned} \tag{45}$$

Sorting this expression in increasing orders of the poles, we get the first term by setting $q = 1$ in the last sum:

$$\sum_{r=1}^{l-1}\left(\sum_{k=1}^{m}\sum_{p\neq k}^{m}\frac{(-1)^{r-1}b_{kr,(l-1)}b_{p1,1}}{(\alpha_k-\alpha_p)^r(s-\alpha_k)}+\sum_{k=1}^{m}\sum_{p\neq k}^{m}\frac{b_{kr,(l-1)}b_{p1,1}}{(\alpha_p-\alpha_k)^r(s-\alpha_p)}\right)$$

Since the last sum above contains all elements except the diagonal elements $k = p$, the indices k and p in that sum can be interchanged. Thus, by extracting the k:th element we get

$$b_{k1,l}=\sum_{r=1}^{l-1}\sum_{p\neq k}^{m}\frac{(-1)^{r-1}b_{kr,(l-1)}b_{p1,1}+b_{pr,(l-1)}b_{k1,1}}{(\alpha_k-\alpha_p)^r},$$

which is equivalent to eqn. (44).

The terms in eqn. (45), having the highest order (l) of the poles, are only contained in the first sum. Thus, setting $r = l-1$ in that sum gives the coefficients $b_{kl,l}$ as defined by eqn. (44).

The remaining coefficients, corresponding to poles of order j, follows from setting $r = j-1$ in the first sum and $q = j$ in the second sum of eqn. (45), noting that only terms for $r \geq j$ contributes, and then extract the k:th element:

$$b_{kj,l}=b_{k(j-1),(l-1)}b_{k1,1}+\sum_{r=j}^{l-1}\sum_{p\neq k}^{m}\frac{(-1)^{r-j}b_{kr,(l-1)}b_{p1,1}}{(\alpha_k-\alpha_p)^{r-j+1}}$$

■

When PFD is carried out on small systems, such as when n and m are small, the coefficients are often found by polynomial identification. The polynomial identification gives a set of linear equations in the nm coefficients. A probably simpler method is to use nm different values ρ, which do not equal any α_k, and calculate the values of $\hat{G}(s)$ with eqn. (28). Eqn. (30) then gives a linear set of nm equations:

$$\begin{bmatrix}
\frac{1}{(\rho_{11}-\alpha_1)} & \cdots & \frac{1}{(\rho_{11}-\alpha_1)^n} & \cdots & \frac{1}{(\rho_{11}-\alpha_k)^j} & \cdots & \frac{1}{(\rho_{11}-\alpha_m)^n} \\
\vdots & & \vdots & & \vdots & & \vdots \\
\frac{1}{(\rho_{1n}-\alpha_1)} & \cdots & \frac{1}{(\rho_{1n}-\alpha_1)^n} & \cdots & \frac{1}{(\rho_{1n}-\alpha_k)^j} & \cdots & \frac{1}{(\rho_{1n}-\alpha_m)^n} \\
\vdots & & \vdots & & \vdots & & \vdots \\
\frac{1}{(\rho_{kj}-\alpha_1)} & \cdots & \frac{1}{(\rho_{kj}-\alpha_1)^n} & \cdots & \frac{1}{(\rho_{kj}-\alpha_k)^j} & \cdots & \frac{1}{(\rho_{kj}-\alpha_m)^n} \\
\vdots & & \vdots & & \vdots & & \vdots \\
\frac{1}{(\rho_{mn}-\alpha_1)} & \cdots & \frac{1}{(\rho_{mn}-\alpha_1)^n} & \cdots & \frac{1}{(\rho_{mn}-\alpha_k)^j} & \cdots & \frac{1}{(\rho_{mn}-\alpha_m)^n}
\end{bmatrix}
\begin{bmatrix} b_{11} \\ \vdots \\ b_{1n} \\ \vdots \\ b_{kj} \\ \vdots \\ b_{mn} \end{bmatrix}
=
\begin{bmatrix} \hat{G}(\rho_{11}) \\ \vdots \\ \hat{G}(\rho_{1n}) \\ \vdots \\ \hat{G}(\rho_{kj}) \\ \vdots \\ \hat{G}(\rho_{mn}) \end{bmatrix}$$

To get numerically accurate solutions bad condition numbers of the nm by nm matrix above must be avoided by a clever choice of the values of ρ.

Both these methods require a solution of nm linear equations, which, in practice, requires n^3m^3 arithmetic operations [5]. By calculating the operations in the recursive algorithm, it is easily verified that the required number of operations is in the order nm^2. Hence, the recursive algorithm requires far less operations.